



## OPEN

SUBJECT AREAS:  
SEISMOLOGY  
GEOPHYSICSReceived  
2 June 2014Accepted  
10 September 2014Published  
30 September 2014Correspondence and  
requests for materials  
should be addressed to  
S.P. (peisp@itpcas.ac.  
cn) or H.Z. (zhang11@  
ustc.edu.cn)

# Ductile Gap between the Wenchuan and Lushan Earthquakes Revealed from the Two-dimensional Pg Seismic Tomography

Shunping Pei<sup>1</sup>, Haijiang Zhang<sup>2</sup>, Jinrong Su<sup>3</sup> & Zhongxiong Cui<sup>1</sup>

<sup>1</sup>Key Laboratory of Continental Collision and Plateau Uplift, Institute of Tibetan Plateau Research, Chinese Academy of Sciences, Beijing 100085, China, <sup>2</sup>Laboratory of Seismology and Physics of Earth's Interior, School of Earth and Space Sciences, University of Science and Technology of China, Hefei, Anhui 230026, China, <sup>3</sup>Seismological Bureau of Sichuan Province, Chengdu 610041, China.

**A high-resolution two-dimensional Pg-wave velocity model is obtained for the upper crust around the epicenters of the April 20, 2013 Ms7.0 Lushan earthquake and the May 12, 2008 Ms8.0 Wenchuan earthquake, China. The tomographic inversion uses 47235 Pg arrival times from 6812 aftershocks recorded by 61 stations around the Lushan and Wenchuan earthquakes. Across the front Longmenshan fault near the Lushan earthquake, there exists a strong velocity contrast with higher velocities to the west and lower velocities to the east. Along the Longmenshan fault system, there exist two high velocity patches showing an “X” shape with an obtuse angle along the near northwest-southeast (NW-SE) direction. They correspond to the Precambrian Pengguan and Baoxing complexes on the surface but with a ~20 km shift, respectively. The aftershock gap of the 2008 Wenchuan and the 2013 Lushan earthquakes is associated with lower velocities. Based on the theory of maximum effective moment criterion, this suggests that the aftershock gap is weak and the ductile deformation is more likely to occur in the upper crust within the gap under the near NW-SE compression. Therefore our results suggest that the large earthquake may be hard to happen within the gap.**

**O**n April 20, 2013, another destructive earthquake with a magnitude of Ms7.0 (or Mw6.6) occurred in Lushan County, China, about 84 km to the southwest of the epicenter of the 2008 Ms8.0 Wenchuan earthquake. The Lushan earthquake is located at longitude 102.966°E and latitude 30.292°N with the depth at 14 km<sup>1</sup>. The same as the 2008 Wenchuan earthquake, the 2013 Lushan earthquake also happened on the Longmenshan fault system, the boundary between the Sichuan basin to the east and the Qiangtang block of the eastern Tibetan Plateau to the west (Figure 1). However, unlike the 2008 Wenchuan earthquake, the Lushan earthquake was initiated along the Pengguan fault while the former one along the Beichuan fault (Figure 1).

This earthquake has a typical thrust-fault focal mechanism<sup>1</sup> with strike/dip/rake of 210°/47°/97°. The pure thrust motion revealed by studies of focal mechanism and rupture process is similar to the southern segment of the rupture process of the Wenchuan earthquake<sup>2–5</sup>. Unlike the Wenchuan earthquake, however, the surface rupture can rarely be indentified, thus it is postulated that the Lushan earthquake occurred on a blind thrust fault<sup>6</sup>. The earthquake ruptures to both ways along the fault but the dominant slip of ~1 m is mainly located to the southwest to the main shock<sup>7</sup>. There are thousands of aftershocks occurring in a zone of ~50 km long along the fault (Figure 1). However, it is noted that along the fault between the Wenchuan and Lushan earthquakes there is a 60-km gap void of aftershocks for both earthquakes (Figure 1).

The occurrence of the Lushan earthquake along the same fault system within 5 years as the Wenchuan earthquake was a surprise to the public as well as to the seismologists although the Coulomb Failure Stress suggests that earthquake hazard on the fault segments where the Lushan earthquake occurred should be enhanced after the Wenchuan earthquake<sup>8</sup>. The same question arised after the Lushan earthquake: when and where will be the next big one along the Longmenshan fault system? Considering the existence of the aftershock gap between the two earthquakes, is it more likely that the next big earthquake will happen there? Knowing the detailed structure of the gap will be helpful for solving this puzzle. Unfortunately, the available seismic velocity models from previous body-wave and surface-wave tomography studies<sup>9–16</sup> for the Longmenshan fault system generally

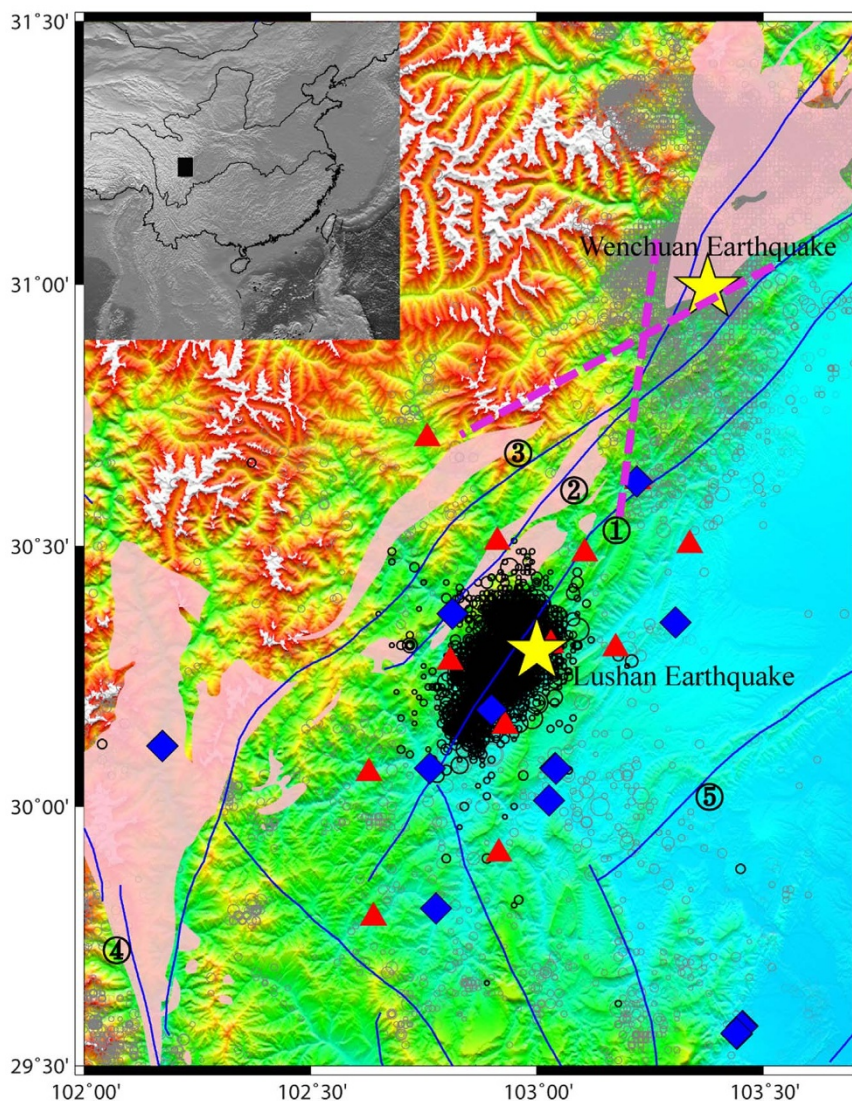


**Figure 1** | Tectonic map around the Lushan and Wenchuan earthquakes (stars). The Longmenshan fault system consisting of faults ①, ②, and ③ marks the boundary between the Sichuan Basin to the east and the eastern Tibetan plateau to the west. The blue lines are active faults<sup>38</sup>. Major faults are: ①Guanxian-Anxian fault; ②Yingxiu-Beichuan fault which is the main Longmenshan fault; ③Wenchuan-Maowen fault; ④Xianshuihe fault; ⑤Pujiang-Xinjin fault. The black circles indicate the aftershocks of the Lushan earthquake and the gray circles are the aftershocks of the 2008 Wenchuan Ms8.0 earthquake. The triangles and diamonds are temporary and permanent stations deployed by Seismological Bureau of Sichuan Province. The pink areas indicate the Precambrian rock bodies on the surface. The inlet map shows the location of the study area. Figure was made using the Generic Mapping Tools<sup>39</sup> version 4.2.1

have a spatial resolution of 50 km or above, too coarse to resolve the detailed structure of the gap. A recent seismic tomography study using the Lushan earthquake aftershocks<sup>17</sup> only resolves the velocity structure around the rupture area, not large enough to cover the aftershock gap region. In this study, we have access to the aftershock data recorded by 15 temporary seismic stations deployed by the Sichuan Seismological Bureau around the Lushan region after the earthquake, along with 26 CEA permanent stations and 20 seismic stations used for monitoring the Zipingpu and Pubugou water reservoirs. The availability of these stations around the Lushan region makes it possible to resolve the detailed velocity structure of the gap region (Figure 2).

**Data.** We collected 47235 Pg arrival times from 6812 aftershocks recorded by 61 stations around the Lushan and Wenchuan earthquake area (Figure 2a). The aftershocks were located using a 1D local velocity model<sup>18</sup> and arrival times were picked from waveforms with a main frequency band of 1 ~ 10 Hz by the

Sichuan Seismological Bureau. For the catalog locations, the location uncertainty in the horizontal plane is generally smaller than 5 km. The arrival time data were selected using the following criteria: each event needs to be recorded by at least 3 stations; each station records at least 3 events; event depth is less than 20 km and the epicentral distance is between 10 km and 200 km. For the selected data, the average epicentral distance is 59 km with a standard deviation of 41 km, and the average focal depth is 14 km with a standard deviation of 4.2 km.

## Results

**Two-dimensional (2D) Pg velocity model.** Here we adopted a recently developed 2D seismic tomography method to determine the 2D Pg velocity model using the aftershock data<sup>19,20</sup>. First by fitting a straight line to the corrected travel times versus epicentral distances according to Equation (2) in the Methods section, an average Pg-wave velocity of 5.75 km/s for the upper crust was obtained from the slope (Figure 2b). The intercept is only

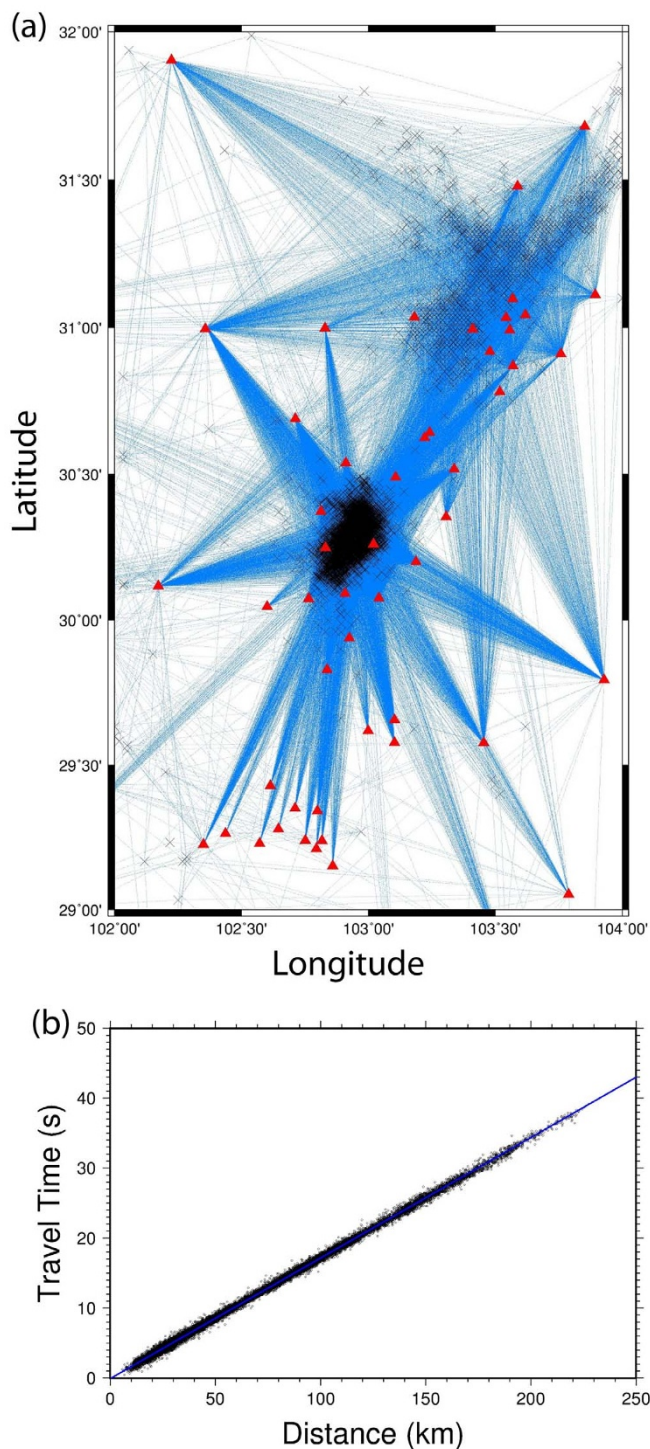


**Figure 2** | (a) Pg ray path coverage and (b) the travel time curves for Pg data used in this study. In total 47235 ray paths were obtained from 6812 events (crosses) recorded on 61 stations (triangles). In the travel time curves, a straight line (blue) with a slope of  $1/5.75$  is found for best fitting the travel time data. Therefore the average Pg is inferred to be 5.75 km/s in this region.

$-0.079$  s, suggesting that the assumption of straight Pg ray paths used in the method is reasonable. For the 2D tomography, the upper crust is discretized into cells of  $2' \times 2'$ . The damped LSQR with a damping value of 200 is applied to the 2D tomographic system to obtain the 2D Pg-wave velocity model, the station correction terms and the event correction terms. After 60 iterations, the standard deviation of travel time residuals decreased from 0.43 s to 0.29 s.

Figure 3 shows the inverted 2D Pg-wave velocity image with aftershocks of magnitude  $> 4.0$  for the Lushan earthquake and historic earthquakes of magnitude  $> 6.0$ . It can be seen that there is a clear velocity contrast across the fault with higher velocity to the west and lower velocity to the east at the epicenter of the Lushan earthquake. This strong seismic velocity contrast across the seismogenic fault was also found in the epicentral area of the Wenchuan earthquake<sup>16,21</sup>. Along the Longmenshan fault system, there exist two high velocity anomalies that form an “X” shape and are spatially consistent with the Precambrian rocks on the surface and with a shift of about 20 km (Figure 3). The locations of the two branches of the “X” shape coincide with the faults or boundaries of the Precambrian complexes (Figure 3). Along the Longmenshan fault system, the aftershock gap is associated with lower velocities compared to the epicentral areas of the Wenchuan and Lushan earthquakes.

**Resolution tests.** Checkerboard resolution tests with different anomaly sizes were conducted to evaluate the model resolution for the selected data. The checkerboard model is created by adding  $\pm 3\%$  anomalies alternatively to the final inverted model with different grid sizes. Travel times are calculated using the same event and station distribution as the real data. Synthetic travel times with the Gaussian

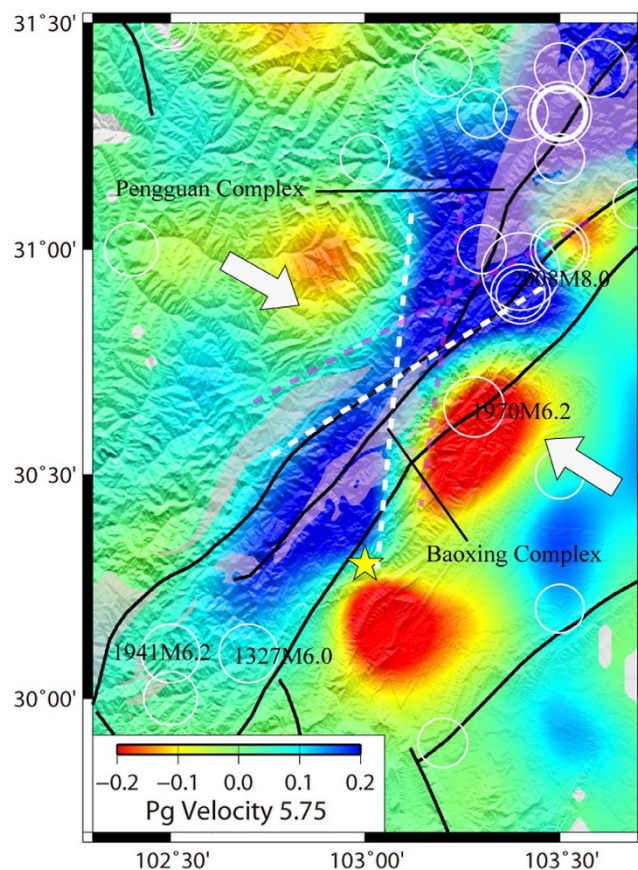


**Figure 3** | The inverted Pg-wave velocity variations with respect to an average velocity of 5.75 km/s. An X shape is clearly seen from two white dashed lines bounding the high velocity anomalies. The pink dashed lines are inferred from the Precambrian Pengguan and Baoxing complexes on the surface. The white arrows indicate the principal compressive stress direction obtained from the focal mechanism analysis. The star shows the epicenter of the Ms7.0 Lushan earthquake. Historic earthquakes (white circles) with magnitudes greater than 5.0 are shown with some earthquakes labeled with year and magnitude. The faults (black lines) are the same as those shown in Figure 1. Figure was made using the Generic Mapping Tools<sup>39</sup> version 4.2.1.



distributed noise of a standard deviation of 0.1 s were used to invert for the checkerboard models with anomaly sizes of  $10' \times 10'$  and  $7.5' \times 7.5'$ . The spatial resolution is considered to be good or reasonable for a region where the checkerboard pattern is recovered. The tests showed that the checkerboard pattern of  $10' \times 10'$  can be recovered for most of the study area while the  $7.5' \times 7.5'$  checkerboard pattern can only be recovered near the epicenter of the Lushan earthquake (Figure 4). Therefore the obtained 2D model has the spatial resolution of  $10' \times 10'$  outside the aftershock zone and  $7.5' \times 7.5'$  resolution near the epicentral area.

The bootstrap technique<sup>22</sup> was also used to assess the robustness of the inversion results. The bootstrap method iteratively re-samples the data pool and re-runs the inversion with the sampled data. The standard deviation in bootstrapped velocities can be used as a proxy for the model uncertainty. For 100 bootstrap inversions, uncertainties in velocity perturbations are found to be less than 0.04 km/s for all cells, which are much smaller than tomographic velocity variations.

## Discussion

A series of complexes along the Longmenshan fault system generally were thought as high-pressure rocks from flux of weak lower crust under the extrusion of Tibetan Plateau<sup>23,24</sup>. Although reverse faulting dominates the deformation of the Longmenshan fault system, right-lateral strike-slip motion also plays an important role in the deformation of complexes. Strike-slip component becomes greater and greater from south to north along the Longmenshan fault system. The Lushan earthquake is dominated by thrust faulting and shows a small component of left lateral strike-slip<sup>25</sup> while the Wenchuan earthquake shows more right-lateral strike-slip at the southern segment of the rupture and becomes near full strike-slip in the northern part. Because of the transition from the pure thrust faulting to the full

strike slip from south to north, the Longmenshan fault system has to be extended along the strike, which may separate the Pengguan complex and Baoxing complex from the entire block. The two complexes are nearly connected in the lower layer of the brittle crust from the tomographic imaging results (Figure 3). However, on the surface they are separated based on the geological mapping. The extension along the Longmenshan fault system is further supported by the normal-fault type focal mechanisms for some aftershocks of the Wenchuan earthquake<sup>26</sup> and opposite tangential crustal movement at two ends of the fault system from the GPS data<sup>27</sup>. A simple geological model is proposed to describe the geodynamic deformation in this region (Figure 5). In this model, Pengguan complex and Baoxing complex are separated in shallow based on the geological features observed on the surface, while they are connected in deep based on the inverted Pg velocity model. The strong compression between the Tibetan Plateau and the Sichuan Basin caused reverse Longmenshan faulting system but with some extension effect along the strike. This extension separates the high-pressure rocks arising from lower crust into isolated Pengguan complex and Baoxing complex on the surface.

After the Lushan earthquake happened, many scientists paid attention to the 60-km aftershock gap between Wenchuan earthquake and Lushan earthquake. Will the gap break out and cause a huge earthquake in the near future? The detailed 2D Pg velocity model shows that the gap is located around the crossing point of the “X” shape and has lower velocities, which is consistent with the coarse-scale tomography models<sup>6,10,12,16</sup>. The Wenchuan and Lushan earthquakes are located at the Yinxiu-Beichuan fault and Guanxian-Anxian fault, namely the central fault and the front fault of the Longmenshan fault system (Figure 1), respectively. They are also located on the two different branches of the “X” shape of the high velocity anomalies, respectively. The angle of the X-shape in the

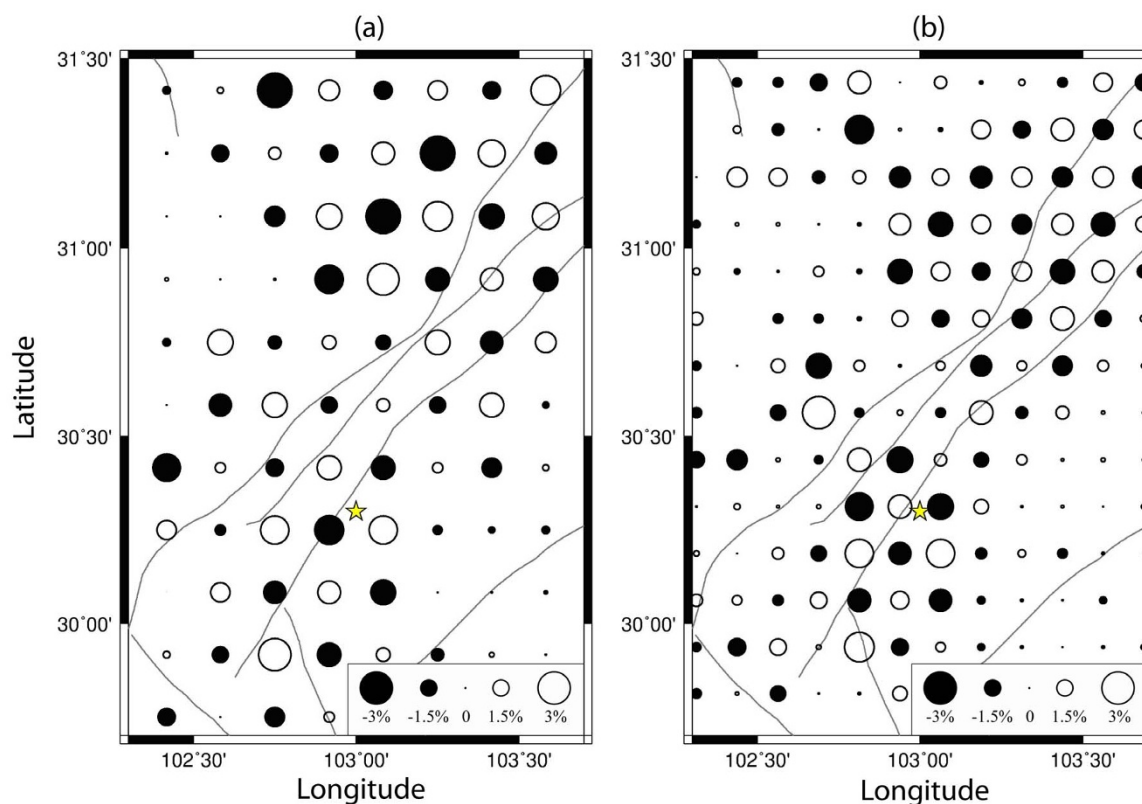


**Figure 4** | Checkerboard resolution tests with different spatial resolutions of (a)  $10' \times 10'$  and (b)  $7.5' \times 7.5'$ . The lines indicate the active faults shown in Figure 1. The empty and filled circles indicate positive and negative velocity anomalies, respectively. Circle sizes represent the recovered checkerboard anomaly amplitude. It shows that the velocity anomalies with a spatial dimension greater than  $10' \times 10'$  can be resolved in the study region with some smearing, and around the epicenter of the Lushan earthquake the velocity model can reach a spatial resolution of  $7.5' \times 7.5'$ .

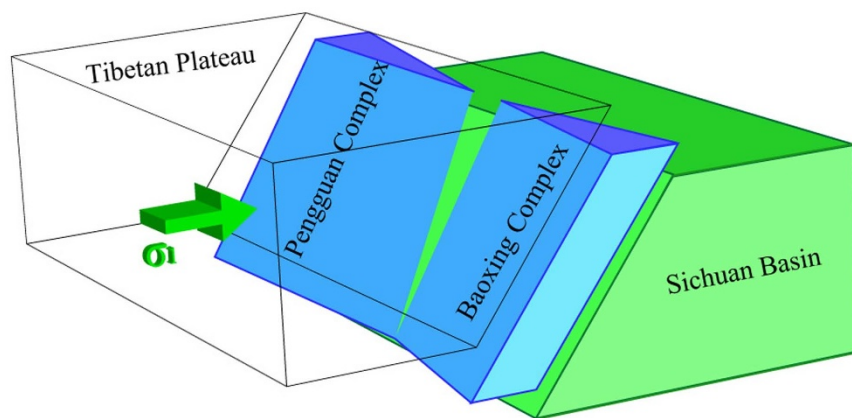


**Figure 5 | The inferred geodynamic model along the Longmenshan fault system.** The Pengguan and Baoxing complexes are connected in the deep region but are separated in the shallow region. The principal compressive direction is denoted by a green arrow.

horizontal maximum compressive direction is obtuse. Based on the theory of maximum effective moment (MEM) criterion<sup>28,29</sup>, in the shortening direction or the maximum compressive direction  $\sigma_1$  the obtuse conjugate angle would be formed under the ductile shear zone otherwise the acute angle would be formed for the brittle shear fractures. According to the MEM criterion, the effective moment  $M_{\text{eff}}$  was represented by  $M_{\text{eff}} = 1/2(\sigma_1 - \sigma_3)\sin(2\alpha)\sin\alpha$  for a unit sample, where  $\alpha$  is the angle between the direction  $\sigma_1$  and the cleavage. For  $\alpha$  within the range of  $54.7 \pm 10^\circ$  the  $M_{\text{eff}}$  reaches maximum or near maximum for all the natural and experimental examples under ductile crenulation<sup>29</sup>. Therefore the obtuse angle ( $2\alpha$ ) of the “X” shape suggests ductile deformation in the upper crust within the gap between the Lushan and Wenchuan earthquakes (Figure 3). Because of the weak and likely ductile nature of the gap, it might act as a barrier for ruptures for both Wenchuan and Lushan earthquakes. The fact that there were very few aftershocks indicates that the aseismic slip likely occurs and thus the stress cannot accumulate within the gap<sup>30,31</sup>. As a result, the gap is hard to break through and produce large earthquakes. This can be used to explain why both Wenchuan and Lushan earthquakes did not rupture this gap and few aftershocks occurred there.

## Methods

In this study, in order to obtain the upper crustal velocity structure around the 2013 Lushan Ms7.0 earthquake and the 2008 Wenchuan Ms8.0 earthquake using their aftershock data recorded by permanent and temporary seismic stations, we applied a recently developed two-dimensional seismic tomography method<sup>19,20</sup>. Compared to the conventional 3D travel time tomography, this 2D method is much simpler with fewer unknowns although it is only suitable for a small region because straight ray paths are assumed.

The Pg travel time residuals are inverted for lateral velocity variations within the seismogenic layer. The observed arrival time of the Pg-wave in the upper crust,  $t_{\text{obs}}$ , can be expressed as the following:

$$t_{\text{obs}} = t + a_{\text{sta}} + b_{\text{evt}}, \quad (1)$$

where  $t$  is the predicted travel time for the Pg ray path through the upper crust according to a reference velocity model, and  $a_{\text{sta}}$  and  $b_{\text{evt}}$  are the station and event correction terms to compensate for the difference between the observed and the predicted time, respectively. The station elevation is also taken into account when calculating the travel time and ray path for the Pg-wave between event and station. The station correction term  $a_{\text{sta}}$  is related to the surface geology and the station clock error, and it compensates for the heterogeneous velocity structure around each station<sup>32</sup>. The event correction term  $b_{\text{evt}}$  mainly takes care of the errors in focal depth and origin time of an earthquake. Because of the trade-off between the focal depth and the origin time, an earlier origin time could be compensated by a deeper source depth and vice versa<sup>33</sup>. Therefore, we here combine these two error terms into one event correction term. Because the uncertainties of event locations in the horizontal plane are relatively small, they are fixed in the inversion. If the Pg wave travels in a nearly homogeneous crust with an average velocity  $v$ , the predicted travel time is simply  $t = \sqrt{h^2 + \Delta^2}/v$  for a straight ray path for an event with a focal depth  $h$  and the epicentral distance  $\Delta$ . Substituting  $t = \sqrt{h^2 + \Delta^2}/v$  in Equation (1) we get

$$t_{\text{obs}} - (\sqrt{h^2 + \Delta^2} - \Delta)/v = \Delta/v + a_{\text{sta}} + b_{\text{evt}}. \quad (2)$$

Usually, the correction term  $(\sqrt{h^2 + \Delta^2} - \Delta)/v$  to the observed travel time on the left-hand side of Equation (2) is small because of  $h \ll \Delta$  for most events. By fitting the corrected travel times versus epicentral distances by a straight line the average upper crust velocity can be estimated. If the crust is further discretized into small 2-D cells, with respect to an average velocity model, we can relate the travel time residuals to the slowness (inverse of velocity) perturbations for cells as follows,

$$t_{ij} = a_i + b_j + \sum_k d_{ijk} \cdot s_k, \quad (3)$$

where  $t_{ij}$  is the travel time residual for the ray from event  $j$  to station  $i$ ,  $a_i$  is the station correction for station  $i$ ,  $b_j$  is the event correction for event  $j$ ,  $d_{ijk}$  is the distance traveled by ray  $ij$  in cell  $k$ , and  $s_k$  is the slowness perturbation for cell  $k$ , respectively. The unknown quantities in the above equation are  $a_i$ ,  $b_j$ , and  $s_k$ .

Damped LSQR<sup>34</sup> with preconditioning is applied to find the least-squares solution of Equation (3)<sup>35,36</sup>. Laplacian smoothing<sup>37</sup> is adopted to regularize the inversion.

- Han, L. *et al.* Focal mechanisms of the 2013 Mw 6.6 Lushan, China earthquake and high-resolution aftershock relocations. *Seism. Res. Lett.* **85**, 8–14 (2014).
- Liu, J. *et al.* Introduction to the Lushan, Sichuan M7.0 earthquake on 20 April 2013. *Chinese J. Geophys.* **56**, 404–4407 (2013).
- Wang, W. M., Hao, J. L. & Yao, Z. X. Preliminary result for rupture process of Apr.20, 2013, Lushan Earthquake, Sichuan. *Chinese J. Geophys.* **56**, 1412–1417 (2013).
- Zeng, X. F., Luo, Y., Han, L. B. & Shi, Y. L. The Lushan Ms7.0 earthquake on 20 April 2013: A high-angle thrust event. *Chinese J. Geophys.* **56**, 1418–1424 (2013).
- Zhang, Y., Xu, L. S. & Chen, Y. T. Rupture process of the Lushan 4.20 earthquake and preliminary analysis on the disaster-causing mechanism. *Chinese J. Geophys.* **56**, 1408–1411 (2013).
- Xu, X. W. *et al.* Lushan MS7.0 earthquake: A blind reserve-fault event. *Chinese Sci. Bull.* **59**, 3437–3443 (2013).
- Hao, J. L., Ji, C., Wang, W. M. & Yao, Z. X. Rupture history of the 2013 Mw 6.6 Lushan earthquake constrained with local strong motion and teleseismic body and surface waves. *Geophys. Res. Lett.* **40**, 5371–5376 (2013).
- Parsons, T., Ji, C. & Kirby, E. Stress changes from the 2008 Wenchuan earthquake and increased hazard in the Sichuan basin. *Nature* **454**, 509–510 (2008).
- Huang, R., Wang, Z., Pei, S. & Wang, Y. Crustal ductile flow and its contribution to tectonic stress in Southwest China. *Tectonophysics* **473**, 476–489 (2009).
- Wang, Z., Fukao, Y. & Pei, S. Structural control of rupturing of the Mw7.9 2008 Wenchuan Earthquake, China. *Earth Planet. Sci. Lett.* **279**, 131–138 (2009).
- Wang, Z. *et al.* Seismic imaging, crustal stress and GPS data analyses: Implications for the generation of the 2008 Wenchuan Earthquake (M7.9), China. *Gondwana Res.* **19**, 202–212 (2010).
- Lei, J. & Zhao, D. Structural heterogeneity and the mechanism of the 2008 Wenchuan earthquake (Ms8.0). *Geochem. Geophys. Geosyst.* **10** (2009).
- Wu, J. P., Huang, Y. & Zhang, T. Z. Aftershock distribution of the Ms8.0 Wenchuan earthquake and three dimensional P-wave velocity structure in and around source region. *Chinese J. Geophys.* **52**, 320–328 (2009).
- Li, C. & van der Hilst, R. D. Structure of the upper mantle and transition zone beneath Southeast Asia from traveltimes tomography. *J. Geophys. Res.* **115** (2010).
- Yang, Y. *et al.* Rayleigh wave phase velocity maps of Tibet and the surrounding regions from ambient seismic noise tomography. *Geochem. Geophys. Geosyst.* **11** (2010).



16. Zhang, H., Roecker, S., Thurber, C. H. & Wang W. *Earth Sciences*. Dar I. A. (ed.) (InTech, Rijeka, 2012).
17. Li, Z., Tian, B., Liu, S. & Yang, J. Asperity of the 2013 Lushan earthquake in the eastern margin of Tibetan Plateau from seismic tomography and aftershock relocation. *Geophys. J. Int.* **195** (2013).
18. Zhao, Z., Fang, J. & Zhen S. Crustal velocity and relocated events in Longmen Shan fault zone. *Acta Seismol. Sin.* **19**, 615–622 (1997).
19. Pei, S. & Chen, Y. J. Link between seismic velocity structure and the 2010 Ms = 7.1 Yushu earthquake, Qinghai, China: Evidence from aftershocks tomography. *Bull. Seism. Soc. Am.* **102**, 445–450 (2012).
20. Pei, S., Chen, Y. J., Feng, B., Gao, X. & Su J. High-resolution seismic velocity structure and azimuthal anisotropy around the 2010 Ms = 7.1 Yushu earthquake, Qinghai, China from 2D tomography. *Tectonophysics*. **584**, 144–151 (2013).
21. Pei, S. *et al.* Three-dimensional seismic velocity structure across the 2008 Wenchuan Ms8.0 earthquake, Sichuan, China. *Tectonophysics* **491**, 211–217 (2010).
22. Hearn, T. M. Anisotropic Pn tomography in the western United States. *J. Geophys. Res.* **101**, 8403–8414 (1996).
23. Burchfiel, B. C., Chen, Z., Liu, Y. & Royden, L. H. Tectonics of the Longmen Shan and adjacent regions, central China. *International Geological Review* **37**, 661–735 (1995).
24. Densmore, A. L. *et al.* Active tectonics of the Beichuan and Pengguan faults at the eastern margin of the Tibetan Plateau. *Tectonics* **26** (2007).
25. Wu, Y. Q. *et al.* Preliminary results of the co-seismic displacement and pre-seismic strain accumulation of the Lushan MS 7.0 earthquake reflected by the GPS surveying. *China Sci. Bull.* **58** (2013).
26. Yi, G. X., Long, F. & Zhang, Z. W. Spatial and temporal variation of focal mechanisms for aftershocks of the 2008 MS8.0 Wenchuan earthquake. *Chinese J. Geophys.* **55**, 1213–1227 (2012).
27. Wang, Q. *et al.* Rupture of deep faults in the 2008 Wenchuan earthquake and uplift of the Longmen Shan. *Nature Geoscience* **4**, 634–640 (2011).
28. Price, N. J. & Cosgrove, J. W. *Analysis of Geological Structures* [1–520] (Cambridge University Press, Cambridge, 1990).
29. Zheng, Y. D., Wang, T., Ma, M. & Davis, G. A. Maximum effective moment criterion and the origin of low-angle normal faults. *J. Struct. l Geol.* **26**, 271–285 (2004).
30. Perfettini, H. *et al.* Seismic and aseismic slip on the central Peru megathrust. *Nature* **465**, 78–81 (2010).
31. Rolandone, F., Bürgmann, R. & Nadeau, R. M. The evolution of the seismic-aseismic transition during the earthquake cycle: Constraints from the time-dependent depth distribution of aftershocks. *Geophys. Res. Lett.* **31** (2004).
32. Pujol, J. Comments on the joint determination of hypocenters and station corrections. *Bull. Seism. Soc. Am.* **78**, 1179–1189 (1988).
33. Bormann, P. *IASPEI New Manual of Seismological Observatory Practice* [Bormann, P. (ed.)] (GeoForschungsZentrum, Potsdam, 2002).
34. Paige, C. C. & Saunders, M. A. LSQR: An algorithm for sparse linear equations and sparse linear system. *ACM Trans. Math. Software* **8**, 43–71 (1982).
35. Pei, S. *et al.* ML Amplitude Tomography in North China. *Bull. Seism. Soc. Am.* **96**, 1560–1566 (2006).
36. Pei, S. *et al.* Upper mantle seismic velocities and anisotropy in China determined through Pn and Sn tomography. *J. Geophys. Res.* **112** (2007).
37. Lees, J. M. & Crosson, R. S. Tomographic inversion for three-dimensional velocity structure at mount St. Helens using earthquake data. *J. Geophys. Res.* **94**, 5716–5728 (1989).
38. Deng, Q. D. *et al.* *Active tectonics map of China* (1 : 400 000 000) (Earthquake Press, Beijing, 2007).
39. Wessel, P. & Smith, W. H. F. New, improved version of the Generic Mapping Tools released. *Eos Trans. AGU* **79**, 579 (1998).

## Acknowledgments

We sincerely thank the Seismological Bureau of Sichuan Province for providing us the data. This research was jointly supported by the NSF of China (Grant Nos. 41174036, 41374091, 41321061), the Chinese Academy of Sciences (Grant No. KZCX2-EW-QN102), and China's State Administration of Foreign Experts Affairs International Partnership Program for Creative Research Teams.

## Author contributions

J.S. and Z.C. were responsible for collecting and processing the data. S.P. conducted the 2D inversion. Both S.P. and H.Z. contributed to interpretation and writing.

## Additional information

**Competing financial interests:** The authors declare no competing financial interests.

**How to cite this article:** Pei, S., Zhang, H., Su, J. & Cui, Z. Ductile Gap between the Wenchuan and Lushan Earthquakes Revealed from the Two-dimensional Pg Seismic Tomography. *Sci. Rep.* **4**, 6489; DOI:10.1038/srep06489 (2014).



This work is licensed under a Creative Commons Attribution-NonCommercial-ShareAlike 4.0 International License. The images or other third party material in this article are included in the article's Creative Commons license, unless indicated otherwise in the credit line; if the material is not included under the Creative Commons license, users will need to obtain permission from the license holder in order to reproduce the material. To view a copy of this license, visit <http://creativecommons.org/licenses/by-nc-sa/4.0/>